arXiv:1403.5756v1 [cond-mat.supr-con] 23 Mar 2014

Non-collinear Andreev reflections in semiconductor nanowires

B. H. Wu,[1,*] W. Yi,[2,3,†] J. C. Cao,[4] and G.-C. Guo[2,3]

[1]*Department of Applied Physics, Donghua University, 2999 North Renmin Road, Shanghai 201620, China*
[2]*Key Laboratory of Quantum Information, University of Science and Technology of China, CAS, Hefei, Anhui, 230026, People's Republic of China*
[3]*Synergetic Innovation Center of Quantum Information and Quantum Physics, University of Science and Technology of China, Hefei, Anhui 230026, China*
[4]*Key Laboratory of Terahertz Solid-State Technology, Shanghai Institute of Microsystem and Information Technology, Chinese Academy of Sciences, 865 Changning Road, Shanghai 200050, China*

We show that non-collinear Andreev reflections can be induced at interfaces of short semiconductor nanowires, where the spin polarizations of the injected and the retro-reflected carriers are typically at an angle which is tunable via system parameters. This peculiar non-collinearity originates from the spin-dependent coupling to in-gap states, which, for appropriate parameters, are related to the tunnel-coupling-induced splitting of Majorana edge states in a finite system. Importantly, we show that previously equivalent microscopic transport processes in a crossed Andreev reflection can be selectively blocked, depending on the voltage configuration, as a result of the non-collinear Andreev reflection. These interesting phenomena can be observed in semiconductor nanowires of experimentally relevant lengths, and are potentially useful for spintronics.

PACS numbers: 74.45.+c, 85.75.-d, 74.78.-w

Introduction.– Andreev reflection (AR) plays a central role in charge transmission at the interface between a normal conductor (N) and a superconductor (S) [1–3]. An important feature of the process is its spin dependence. Near the interface, an electron with certain spin injected from N is retro-reflected as a hole of the opposite spin via a conventional local Andreev reflection (LAR). However, for situations where spin-flip is allowed at the interface, equal spin AR can take place, where both the electron and the hole have the same spin [4, 5]. Recently, it has been shown that spin-dependent AR can be induced by the Majorana bound state (MBS) residing on the edges of topological superconducting nanowire due to its self-Hermitian nature [6, 7]. However, for a short nanowire, this self-Hermitian property does not hold due to the tunnel-coupling between MBSs on the edges. As a result, the spin-dependence of the AR is bound to be affected in finite-size systems.

For a finite-length nanowire with spin-orbit coupling, Zeeman splitting and proximity-induced superconductivity, pairs of non-degenerate discrete states [8] would appear in the superconducting gap. In this work, we show that electrons and holes involved in a resonant AR [9, 10] with these in-gap states can have tunable and non-collinear spin orientations, in contrast to the conventional or the equal spin AR. This peculiar non-collinear AR is related to the non-collinearity of the local spin polarizations of electrons and holes at the wire ends, which are tunable via parameters such as the Zeeman splitting, the spin-orbit coupling and wire length.

The effect of non-collinear AR is particularly manifest for the crossed Andreev reflection (CAR) in short nanowires, where the distance between the leads is comparable to the superconducting coherence length. Microscopically, the CAR has been understood, analogous to the LAR, as a process involving electron-hole transport, where an electron is injected from one lead while a hole exits to the other [9–17]. As the propagation of electrons is equivalent to the counter-propagation of holes with the same spin, an alternative picture is that of the electron-electron transport, where two spatially separated electrons are respectively injected from the two leads [10, 16, 17]. However, as shown in the following, these two pictures are no longer equivalent as electrons and holes involved in the CAR can have non-collinear

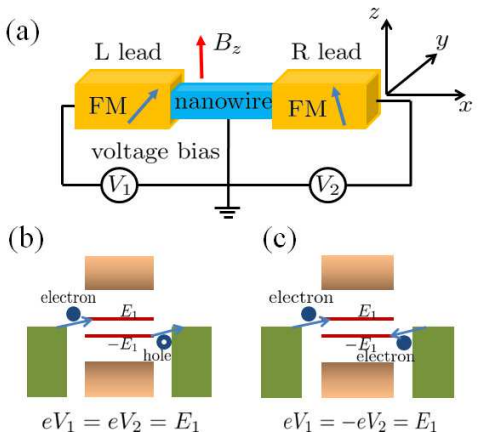

FIG. 1: (a) Schematic plot of the device where a semiconductor nanowire with proximity-induced superconductivity is coupled to two leads. A Zeeman field B_z in the z-direction is applied. Schematic plots of microscopic processes in a resonant CAR are given in (b) and (c).

spin orientations.

A paradigm scenario where the aforementioned pictures of the CAR can be distinguished is by placing two ferromagnetic (FM) leads in contact with the nanowire (see Fig. 1). We show that the microscopic transport processes of the CAR can be selectively blocked, depending on the voltage configuration. More specifically, when the Fermi levels of the two leads are aligned with the same in-gap state, an injected electron is accompanied by an outgoing hole in the CAR (Fig. 1b), while electron-electron transport is blocked; in contrast, when the Fermi levels of the two leads are each aligned with a different in-gap state, two electrons are injected from the leads while electron-hole transport is blocked (Fig. 1c). We show that these fundamental differences can leave signatures in the differential conductance and the noise Fano factor, which can be probed experimentally.

Model.– We consider a quasi-one-dimensional semiconductor nanowire, which has been shown to host MBS for appropriate parameters [18]. As illustrated in Fig. 1a, the wire lies in the x-direction with an external magnetic field B_z along the z-direction. The two ends of the nanowire are tunnel-coupled respectively to the left (L) and the right (R) leads. The wire is grounded while the chemical potentials of the two leads can be tuned, respectively, by applying voltages V_1 and V_2.

In the tight-binding form, the Hamiltonian for the nanowire $H_{\rm wire}$ reads [19, 20]

$$H_{\rm wire} = \sum_{j=1}^{N-1}\left(-\frac{t_0}{2}c_j^\dagger c_{j+1} - \frac{\alpha_{\rm SO}}{2}ic_j^\dagger\sigma_y c_{j+1} + H.c.\right) + \sum_{j=1}^{N}\left[V_z c_j^\dagger\sigma_z c_j - (\mu - t)c_j^\dagger c_j + \Delta(c_{j\uparrow}c_{j\downarrow} + H.c.)\right], \quad (1)$$

where $c_j = (c_{j\uparrow}, c_{j\downarrow})^T$ is the annihilation operator in spinor form for electrons at site j with spin up ($\uparrow$) and down ($\downarrow$) in the z-direction, N is the number of the lattice sites, $\sigma_{y,z}$ are the Pauli matrices, $\alpha_{SO} = \alpha_R/a$ is the spin-orbit coupling constant, with the Rashba parameter α_R and the lattice spacing a, V_z is the effective Zeeman field, Δ is the proximity-induced superconducting gap, and μ is the chemical potential. The hopping rate $t_0 = \frac{\hbar^2}{m^* a^2}$, and m^* is the effective mass of electrons.

The FM leads are described by the mean-field Stoner model [21] as

$$H_{\rm lead} = \sum_{\alpha k s}\epsilon_{\alpha k s}a_{\alpha k s}^\dagger a_{\alpha k s}, \quad (2)$$

where $a_{\alpha k s}$ is the annihilation operator with quantum number k, spin index s and energy $\epsilon_{\alpha k s}$ in the α =L,R lead. Here, $s = +(-)$ denotes spins parallel (anti-parallel) to the FM magnetic moment $\boldsymbol{n}_\alpha = (\sin\theta_\alpha\cos\varphi_\alpha, \sin\theta_\alpha\sin\varphi_\alpha, \cos\theta_\alpha)$, where θ_α and φ_α are the azimuthal angles in the α lead.

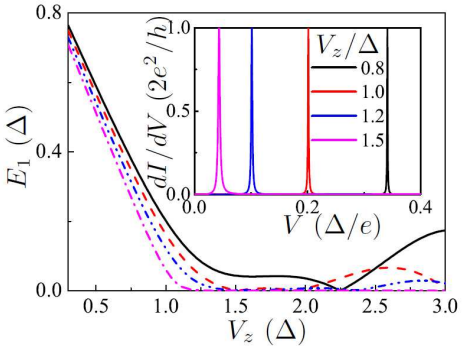

FIG. 2: The lowest discrete state energy E_1 of the wire as a function of the effective Zeeman field V_z for wire length $L = 1.2$ μm (solid line), $L = 1.5$ μm (dashed line), $L = 2.1$ μm (dash dot dot line) and $L = 4.5$ μm (dash dot line). The inset: differential conductance dI/dV at various V_z. Parameters for the inset: $L = 1.2$ μm, $\Gamma_L^\pm = 0.2$ t_0.

The coupling between the leads and the nanowire is given by

$$H_T = \sum_k (t_L c_1^\dagger u_L a_{Lk} + h.c.) + \sum_k (t_R c_N^\dagger u_R a_{Rk} + h.c.), \quad (3)$$

where t_α is the hopping between the α lead and the wire, the electron annihilation operators in spinor form $a_{\alpha k} = (a_{\alpha k+}, a_{\alpha k-})^T$. The unitary matrix u_α [22] accounts for the misalignment of the magnetic moment in the α lead with the z-direction as

$$u_\alpha = \begin{pmatrix} \cos\theta_\alpha/2 & e^{-i\varphi_\alpha}\sin\theta_\alpha/2 \\ e^{i\varphi_\alpha}\sin\theta_\alpha/2 & -\cos\theta_\alpha/2 \end{pmatrix}. \quad (4)$$

The coupling strength between electrons and the α lead is given by $\Gamma_\alpha^s = 2\pi t_\alpha^2\rho_\alpha^s$ ($s = \pm$), where ρ_α^s is the density of states (DOS) in the corresponding lead. In the wide-band limit, Γ_α^s becomes energy-independent. The Stoner model for the FM is characterized by the spin asymmetry in the DOS for the majority ($s = +$) and minority ($s = -$) spins. In particular, for a normal lead, we have $\Gamma_\alpha^+ = \Gamma_\alpha^-$ while for fully spin-polarized FM or half metal (HM) leads, $\Gamma_\alpha^- = 0$.

We are interested in the transport properties of the system. The current operator for the L lead is related to the evolution of the charge carrier number $N_L = \sum_{ks} a_{Lks}^\dagger a_{Lks}$ as $\hat{I} = -e\dot{N}_L$[23]. Much information can be obtained from the current fluctuation or noise due to the discrete nature of charge transport [24]. Here, we focus on the autocorrelation of the current from the L lead. The zero-frequency noise spectral density is defined as $S = \hbar\int dt'\langle\delta I(t')\delta I(0) + \delta I(0)\delta I(t')\rangle$, where $\delta I(t') = \hat{I}(t) - I$ with $I = \langle\hat{I}\rangle$ the dc current from the L lead. Both the current and the noise spectral density can be evaluated by the standard Keldysh Green's function method [25].

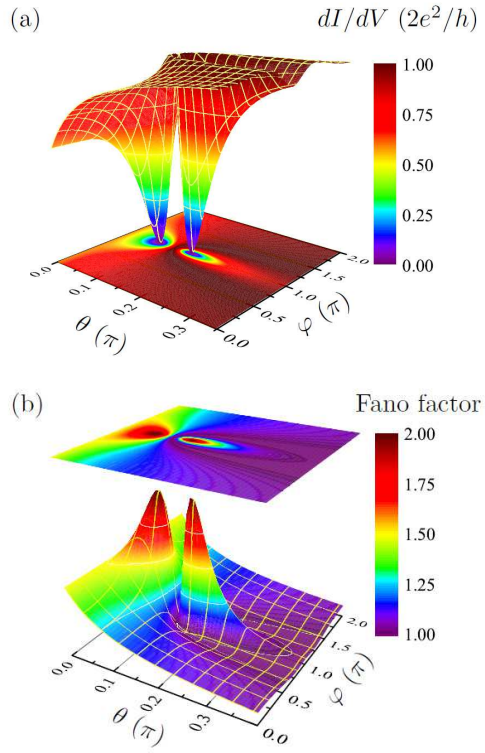

FIG. 3: Contour plots of The differential conductance dI/dV (a) and noise Fano factor (b) due to resonant LAR as functions of azimuth angles θ and φ of the HM magnetic moment. Parameters: $V_z = 1.2\ \Delta$, $\Gamma_L^+ = 0.4\ t_0$, $L = 1.2\ \mu$m.

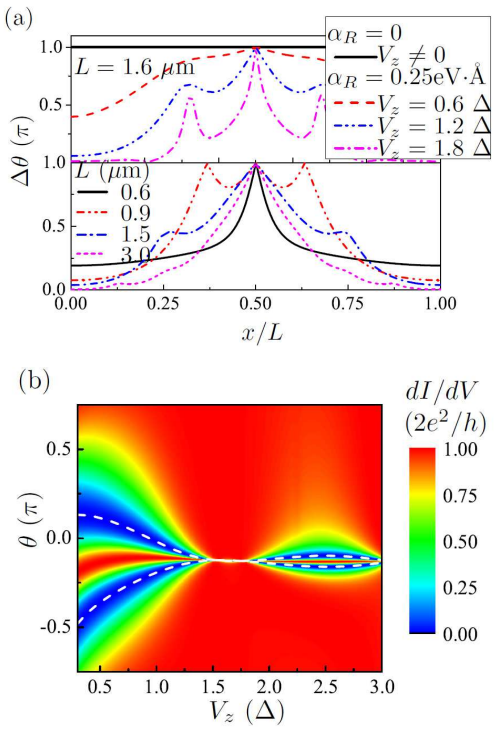

FIG. 4: (a) The spatial dependence of $\Delta\theta$, the angle for the local spin orientations of electron and hole component of the lowest discrete state for system parameters such as V_z, α_R and L. (b) Contour plot of the differential conductance dI/dV as function of V_z and the azimuth angle θ of the magnetic moment in the HM lead. The dashed lines in (b) indicate the directions opposite to the spin orientation of electrons and holes on edge of the wire. Parameters without other statement: $\Gamma_L^+ = 0.4\ t_0$, $V_z = 1.2\ \Delta$, $L = 1.2\ \mu$m and $\alpha_R = 0.25$ eV $\cdot$ Å.

For numerical simulations, we consider a heterostructure in which InSb nanowire is in contact with NbTiN [26, 27]. Following the experiments, we choose typical parameters as: $m^* = 0.015m_e$, with m_e the electron mass, $\alpha_R = 0.25$ eV·Å , $a = 1$nm and $\Delta \sim 140\ \mu$eV. The chemical potential of the wire is chosen as the zero energy reference and the temperature is assumed zero. We will show non-collinear AR can be detected in nanowires ranging from submicron to several microns in length.

In-gap states and local Andreev reflection.– As the resonant AR is typically connected with the discrete states in the superconducting gap, we first characterize the behavior of the lowest in-gap states in a finite-size system, which, under particle-hole symmetry, emerge in pairs with the same energy spacing E_1 to the chemical potential. We show in Fig. 2 the non-monotonic evolution of E_1 as a function of V_z [8]. The existence of discrete in-gap states can be probed by the transport measurement. In the inset of Fig. 2, we show the differential conductance dI/dV as a function of V_z, with an N lead coupled to the L end of the wire, where the dominant transport process is LAR. When the Fermi level of the lead is aligned with the in-gap state, clear signatures of resonant LAR can be identified, where the peak conductance approaches $2e^2/h$.

Signatures of non-collinear AR can be identified by replacing the N lead with an HM lead while the bias voltage V satisfies the condition for resonant AR. We plot the differential conductance dI/dV in Fig. 3a as a function of the azimuthal angles θ and φ of the HM magnetic moment. In most situations, dI/dV approaches $2e^2/h$ due to resonant LAR. However, two dips at some particular spin polarizations can be identified in Fig. 3a, indicating a complete suppression of resonant LAR. As electrons and holes with their spin anti-parallel to the magnetic moment of the HM are effectively blocked, the two dips of dI/dV then suggest a non-collinear LAR where the spin-polarizations of the injected electron/hole and the retro-reflected electron/hole are not aligned. The suppression of LAR can also be revealed by the current noise Fano factor $F = S/2eI$ [24, 28, 29]. For the LAR-dominated transport, the Fano factor approaches 2 at low transmission, indicating an effective transfer of two electrons in the process [10]. In Fig. 3b, two such peaks emerge in the contour plot of F, which are consistent with those of the dips in Fig. 3a, suggesting blocked LAR.

This blocking of LAR originates from the unavailability of either electron or hole with non-collinear spins involved in the resonant LAR. It is instructive to explore the local electron/hole spin orientation $\vec{s}_{e/h}(x)$, which is defined by

$$\vec{s}_{e/h}(x) = \frac{\langle \psi_{e/h}(x) \mid \vec{\sigma} \mid \psi_{e/h}(x) \rangle}{\langle \psi_{e/h}(x) \mid \psi_{e/h}(x) \rangle}, \tag{5}$$

where $\psi_{e/h}(x)$ is a spinor for the one-dimensional electron/hole component of the wave function. $\vec{\sigma}$ is a vector of Pauli matrices.

In Fig. 4a, we plot the spatial dependence of the angle $\Delta\theta$, between $\vec{s}_e$ and $\vec{s}_h$. While the spin orientations of electron and hole components are collinear ($\Delta\theta = \pi$) in the absence of spin-orbit coupling ($\alpha_R = 0$ in the upper panel), they become non-collinear under finite spin-orbit coupling. In particular, $\Delta\theta$ at the wire end can be tuned by adjusting α_R, V_z and L. With increasing L, $\Delta\theta$ at the wire end decreases, approaching zero in the semi-infinite limit, leading to an equal spin AR [6]. We will show that the spin-dependence of AR is intimately connected to these local spin orientations.

We consider the situation where an HM lead is attached to the L end of the wire. We fix the magnetic moment of the lead in the $x - z$ plane, and adopt the convention: $\theta > 0$ for $\varphi = 0$ while $\theta < 0$ for $\varphi = \pi$. In Fig. 4b, we show the contour plot of the differential conductance dI/dV as a function of θ and V_z, for which the voltage $V = E_1$ is applied to enable resonant LAR. Clearly, the directions opposing the spin orientations of electrons and holes at the outmost site (dashed) overlap with the dI/dV dips. These results suggest that once the HM magnetic moment is anti-parallel to the local spin orientation of either electron or hole at the wire end, the resonant LAR can be effectively suppressed since the transport channel for either electron injection or hole retro-reflection is blocked.

Crossed Andreev reflection.– In the following, we show that the non-collinear AR can have highly non-trivial implications for the CAR, which dominates the charge transfer in short nanowires with two terminals [9–11]. To investigate the spin-dependence in the CAR, two HM leads are symmetrically attached to the nanowire. With the wire ends fixed at $x = 0$ and $x = L$, the Hamiltonian of the wire respects the symmetry: $H(x, \alpha) = H(L - x, -\alpha)$. The local spin orientation of the carriers then satisfy: $s^{x,y}_{e/h}(x) = -s^{x,y}_{e/h}(L - x)$ and $s^{z}_{e/h}(x) = s^{z}_{e/h}(L - x)$. This symmetry is useful to distinguish the microscopic transport processes in a non-collinear CAR, which have been assumed to be equivalent the conventional or equal spin CAR. The exact microscopic picture depends on the voltage configuration.

We first consider identical bias voltages $eV_1 = eV_2 = E_1$ where the Fermi levels of both leads are aligned with the same in-gap state. As demonstrated in Fig. 5a, by varying the spin orientations of the L and R leads in the $x - z$ plane, two broad humps, each with a sharp feature peaked close to 2, appear in the noise Fano factor. These peaks show that the transport is LAR-dominated, in contrast to a CAR-dominated transport where F approaches 1 at low transmission. Moreover, the peak positions satisfy $\theta_L = -\theta_R$, suggesting the simultaneous blocking of the same-type carrier injection from the two leads according to the aforementioned symmetry. This shows that the maximal suppression of the CAR occurs when neither electrons nor holes of the desired spin orientation are available from the leads. The microscopic picture for the CAR can then be understood as the incident of an electron from one lead while a hole is emitted to the other, as shown in Fig. 1b.

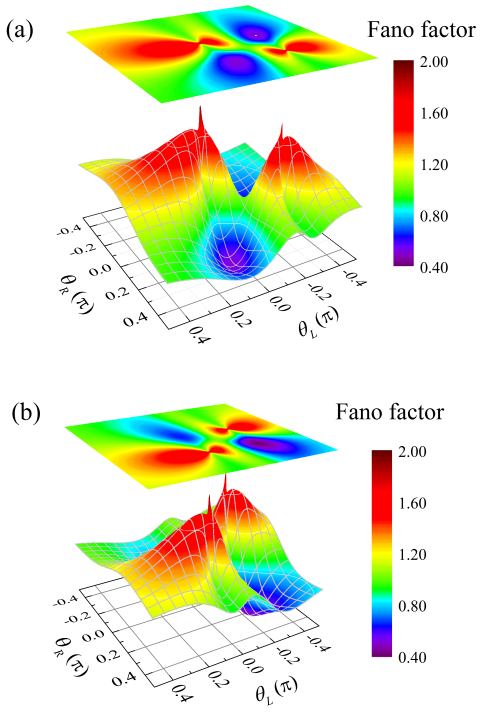

FIG. 5: The contour plots of the noise Fano factor F as functions of θ_L and θ_R for different bias configurations for the resonant CAR: (a) $eV_1 = eV_2 = E_1$ and (b) $eV_1 = -eV_2 = E_1$. Parameters: $V_z = 0.8\ \Delta$, $\Gamma^+_\alpha = 0.4\ t_0$, $L = 1.2\ \mu$m.

Next, we consider bias voltages $eV_1 = -eV_2 = E_1$, under which the Fermi levels of the two leads are aligned, respectively, to a pair of in-gap states. The contour plot of the noise Fano factor measured at the L lead is shown in Fig. 5b. Again, we find two sharp peaks, with peak values close to 2, suggesting the suppression of transmission in resonant CAR. However, the positions of the two peaks are quite different from those in Fig. 5a. Here, the noise peaks appear when the electron channel in one lead and the hole channel in the other are simultaneously blocked. The microscopic picture for the CAR here can

then be understood as the simultaneous injection (emission) of one electron (hole) from each lead to for a Cooper pair, which is schematically shown in Fig. 1c.

The bias voltage dependence of the microscopic transport processes of the CAR can be understood as the following. When an electron or hole tunnels between a biased lead and the in-gap state, it gains or loses energy depending on its charge and the voltage difference across the interface. As the nanowire is grounded, electrons or holes must have zero total energy in forming Cooper pairs. As a result, the carriers involved in the CAR will be highly sensitive to the voltage configuration. Different from the conventional or equal spin AR, the non-collinear AR then allows us to tell apart the underlying microscopic pictures. This feature also provides us with a useful tool to selectively induce fully spin-polarized electron or hole current for applications in spintronics.

Conlusions.– In summary, we have shown that non-collinear AR can be induced at interfaces of semiconductor nanowires of finite, but experimentally relevant length. This peculiar non-collinearity originates from the spin-dependent coupling to the in-gap states which, for appropriate parameters, are related to the tunnel-coupling-induced splitting of Majorana edge states in a finite system. The microscopic pictures which are previously assumed equivalent for the CAR can now be distinguished by the transport properties under different voltage configuration. These interesting phenomena can be observed in semiconductor nanowires with strong spin-orbit coupling, such as InSb [26, 27] or InAs [30], which are currently of intense interest for the search of MBS. A test of the non-collinear AR via transport properties is also within the reach of present technology, where supercurrent through HM films such as CrO_2 has recently been reported [31].

Acknowledgement.– The authors are grateful for helpful discussions with Kam Tuen Law, Xiongjun Liu, Carsten Timm, Philip Brydon and Yuval Ronen. This work is supported by NFRP (2011CB921200, 2011CBA00200), NNSF (60921091), the Natural Science Foundation of China (11074266,11105134,11374283) and the Fundamental Research Funds for the Central Universities (WK2470000006).

* Electronic address: bhwu2010@gmail.com
† Electronic address: wyiz@ustc.edu.cn

[1] A. F. Andreev, Sov. Phys. JETP **19**, 1228 (1964).
[2] G. E. Blonder, M. Tinkham, and T. M. Klapwijk, Phys. Rev. B **25**, 4515 (1982).
[3] M. Tinkham, *Introduction to Superconductivity*, 2nd ed. (Dover, New York, 2004).
[4] Z. P. Niu, Europhys. Lett. **100**, 17012 (2012).
[5] C. Visani, Z. Sefrioui, J. Tornos, C. Leon, J. Briatico, M. Bibes, A. Barthélémy, J. Santamaria, and J. Villegas, Nat. Phys. **8**, 539 (2012).
[6] J. J. He, T. K. Ng, P. A. Lee, and K. T. Law, Phys. Rev. Lett. **112**, 037001 (2014).
[7] J. J. He, J. S. Wu, T. P. Choy, X. J. Liu, Y. Tanaka, and K. T. Law, Nat. Commun. **5**, 3232 (2014).
[8] T. D. Stanescu, R. M. Lutchyn, and S. Das Sarma, Phys. Rev. B **87**, 094518 (2013).
[9] J. Nilsson, A. R. Akhmerov, and C. W. J. Beenakker, Phys. Rev. Lett. **101**, 120403 (2008).
[10] K. T. Law, P. A. Lee, and T. K. Ng, Phys. Rev. Lett. **103**, 237001 (2009).
[11] J. Liu, F.-C. Zhang, and K. T. Law, Phys. Rev. B **88**, 064509 (2013).
[12] J. M. Byers and M. E. Flatté, Phys. Rev. Lett. **74**, 306 (1995).
[13] G. Deutscher and D. Feinberg, Appl. Phys. Lett. **76**, 487 (2000).
[14] M. S. Choi, C. Bruder and D. Loss, Phys. Rev. B **62**, 13569 (2000).
[15] G. B. Lesovik, T. Martin, and G. Blatter, Eur. Phys. J. B **24**, 287 (2001).
[16] J. Linder and A. Sudbø, in *Nanoscience and Engineering in Superconductivity*, edited by V. Moshchalkov, R. Wördenweber, and W. Lang (Springer, Berlin-Heidelberg, 2010).
[17] M. S. Kalenkov and A. D. Zaikin, in *Fundamentals of Superconducting Nanoelectronics*, edited by A. Sidorenko (Springer, Berlin-Heidelberg, 2011).
[18] Y. Oreg, G. Refael, and F. von Oppen, Phys. Rev. Lett. **105**, 177002 (2010).
[19] E. M. Stoudenmire, J. Alicea, O. A. Starykh, and M. P. A. Fisher, Phys. Rev. B **84**, 014503 (2011).
[20] B. H. Wu and J. C. Cao, Phys. Rev. Lett. **85**, 085415 (2012).
[21] Z. Y. Zeng, B. Li, and F. Claro, Phys. Rev. B **68**, 115319 (2003).
[22] J. C. Chen, S. G. Cheng, S. Q. Sun and Q. F. Sun, J. Phys.:Condens. Matter **22**, 035301 (2010).
[23] H. Haug and A.-P. Jauho, *Quantum Kinetics in Transport and Optics of Semiconductors*, 2nd ed. (Springer, Berlin, 2008).
[24] Ya. M. Blanter and M. Büttiker, Phys. Rep. **336**, 1 (2000).
[25] See Supplementary Material for detailed formalism for the calculation of current and noise spectral density.
[26] V. Mourik, K. Zuo, S. M. Frolov, S. R. Plissard, E. P. A. M. Bakkers, and L. P. Kouwenhoven, Science **336**, 1003 (2012).
[27] M. T. Deng, C. L. Yu, G. Y. Huang, M. Larsson, P. Caroff, and H. Q. Xu, Nano Lett. **12**, 6414 (2012).
[28] D. Averin and H. T. Imam, Phys. Rev. Lett. **76**, 3814 (1996).
[29] J. C. Cuevas, A. Martin-Rodero, and A. L. Yeyati, Phys. Rev. Lett. **82**, 4086 (1999).
[30] A. Das, Y. Ronen, Y. Most, Y. Oreg, M. Heiblum, and H. Shtrikman, Nat. Phys. 8, 887 (2012).
[31] R. S. Keizer, S. T. B. Goennenwein, T. M. Klapwijk, G. Miao, G. Xiao, and A. Gupta, Nature **439**, 825 (2006).

Supplementary material

In this Supplementary material, we present the formalism for the calculation of the current and the noise spectral density. The transport properties such as the differential conductance and current noise can be obtained by the Green's function method. The current from the L lead is given by

$$I = \frac{e}{h}\int d\epsilon \mathrm{ReTr}\left\{\hat{\boldsymbol{\sigma}}\left[\boldsymbol{G}^{<}\boldsymbol{\Sigma}^{a}_{1,1} + \boldsymbol{G}^{r}\boldsymbol{\Sigma}^{<}_{1,1}\right]\right\}, \tag{6}$$

where $\hat{\boldsymbol{\sigma}} = \mathrm{diag}(1,-1,1,-1)$ in the spin⊗Nambu space accounts for the different charge carried by electrons and holes. The retarded (lesser) Green's function $\boldsymbol{G}^{r/<}$ can be derived from the analytical continuation of the contour-ordered Green's function $\boldsymbol{G}(t,t') = -i\langle T\psi(t)\psi^{\dagger}(t')\rangle$, where $\psi_j = (c_{j\uparrow}, c^{\dagger}_{j\downarrow}, c_{j\downarrow}, c^{\dagger}_{j\uparrow})^T$. The retarded (advanced) self-energy $\boldsymbol{\Sigma}^{r/a}$ with the relation $\boldsymbol{\Sigma}^{r} = (\boldsymbol{\Sigma}^{a})^{\dagger}$ has non-zero elements for lattice sites at the ends of the wire due to the tunnel-coupling. In the wide-band limit, $\boldsymbol{\Sigma}^{r}$ for the outmost sites is given by $\boldsymbol{\Sigma}^{r}_{1,1} = -i\boldsymbol{\Gamma}_L/2$ and $\boldsymbol{\Sigma}^{r}_{N,N} = -i\boldsymbol{\Gamma}_R/2$, where the matrix $\boldsymbol{\Gamma}_{\alpha}$ is given in spin⊗Nambu space as

$$\boldsymbol{\Gamma}_{\alpha} = \begin{pmatrix} \gamma_{11} & 0 & \gamma_{12} & 0 \\ 0 & \gamma_{22} & 0 & \gamma_{21} \\ \gamma_{21} & 0 & \gamma_{22} & 0 \\ 0 & \gamma_{12} & 0 & \gamma_{11} \end{pmatrix}.$$

Here, $\gamma_{11} = \Gamma^{+}_{\alpha}\cos^2\frac{\theta_{\alpha}}{2} + \Gamma^{-}_{\alpha}\sin^2\frac{\theta_{\alpha}}{2}$, $\gamma_{22} = \Gamma^{+}_{\alpha}\sin^2\frac{\theta_{\alpha}}{2} + \Gamma^{-}_{\alpha}\cos^2\frac{\theta_{\alpha}}{2}$, $\gamma_{12} = (\Gamma^{+}_{\alpha}e^{-i\varphi_{\alpha}} - \Gamma^{-}_{\alpha}e^{i\varphi})\frac{\sin\theta_{\alpha}}{2}$ and $\gamma_{21} = \gamma^{*}_{12}$. The lesser self-energy $\boldsymbol{\Sigma}^{<}$ which characterizes the particle injection from the leads are given by $\boldsymbol{\Sigma}^{<} = [\boldsymbol{\Sigma}^{a} - \boldsymbol{\Sigma}^{r}]\,\boldsymbol{F}$, where $\boldsymbol{F}_{1,1} = \mathrm{diag}(f(\epsilon-\mu_L), f(\epsilon+\mu_L), f(\epsilon-\mu_L), f(\epsilon+\mu_L))$ and $\boldsymbol{F}_{N,N} = \mathrm{diag}(f(\epsilon-\mu_R), f(\epsilon+\mu_R), f(\epsilon-\mu_R), f(\epsilon+\mu_R))$ with f the Fermi distribution function.

In this work, we focus on the autocorrelation of the current from the L lead. The zero-frequency noise spectral density is defined as $S = \hbar\int dt'\langle\delta I(t')\delta I(0) + \delta I(0)\delta I(t')\rangle$, where $\delta I(t') = \hat{I}(t) - I$ is the current fluctuation. $\hat{I}$ is the current operator. In terms of the Green's functions and self-energies, the noise spectral density can be obtained from

$$\begin{aligned} S = \frac{e^2}{h}\int d\epsilon \mathrm{Tr}\Big\{ & \left[\hat{\boldsymbol{\sigma}}\boldsymbol{\Sigma}^{<}_{1,1}\hat{\boldsymbol{\sigma}}\boldsymbol{G}^{>} + \boldsymbol{G}^{<}\hat{\boldsymbol{\sigma}}\boldsymbol{\Sigma}^{>}_{1,1}\hat{\boldsymbol{\sigma}}\right] \\ & -\hat{\boldsymbol{\sigma}}\left[\boldsymbol{\Sigma}_{1,1}\boldsymbol{G}\right]^{<}\hat{\boldsymbol{\sigma}}\left[\boldsymbol{\Sigma}_{1,1}\boldsymbol{G}\right]^{>} - \left[\boldsymbol{G}\boldsymbol{\Sigma}_{1,1}\right]^{<}\hat{\boldsymbol{\sigma}}\left[\boldsymbol{G}\boldsymbol{\Sigma}_{1,1}\right]^{>}\hat{\boldsymbol{\sigma}} \\ & +\boldsymbol{G}^{>}\hat{\boldsymbol{\sigma}}[\boldsymbol{\Sigma}_{1,1}\boldsymbol{G}\boldsymbol{\Sigma}_{1,1}]^{<}\hat{\boldsymbol{\sigma}} + \hat{\boldsymbol{\sigma}}[\boldsymbol{\Sigma}_{1,1}\boldsymbol{G}\boldsymbol{\Sigma}_{1,1}]^{>}\hat{\boldsymbol{\sigma}}\boldsymbol{G}^{<}\Big\}, \end{aligned} \tag{7}$$

where the Langreth theorem of analytic continuation such as $[AB]^{\lessgtr} = A^{r}B^{\lessgtr} + A^{\lessgtr}B^{a}$ and $[ABC]^{\lessgtr} = A^{r}B^{r}C^{\lessgtr} + A^{r}B^{\lessgtr}C^{a} + A^{\lessgtr}B^{a}C^{a}$, have been employed. In the above expressions, the advanced Green's function $\boldsymbol{G}^{a} = (\boldsymbol{G}^{r})^{\dagger}$ and the greater Green's function $\boldsymbol{G}^{>}$ can be found from the relation $\boldsymbol{G}^{>} - \boldsymbol{G}^{<} = \boldsymbol{G}^{r} - \boldsymbol{G}^{a}$.